



Type Three Secretion System-Dependent Microvascular Thrombosis and Ischemic Enteritis in Human Gut Xenografts Infected with Enteropathogenic *Escherichia coli*

Einat Nissim-Eliraz,^a Eilam Nir,^a Irit Shoval,^a Noga Marsiano,^a Israel Nissan,^a Hadar Shemesh,^a Nandor Nagy,^{b,c} Allan M. Goldstein,^b Michael Gutnick,^a Ilan Rosenshine,^d Simcha Yagel,^e  Nahum Y. Shpigel^a

The Koret School of Veterinary Medicine, The Hebrew University of Jerusalem, Rehovot, Israel^a; Department of Pediatric Surgery, Massachusetts General Hospital, Harvard Medical School, Boston, Massachusetts, USA^b; Department of Anatomy, Histology, and Embryology, Faculty of Medicine, Semmelweis University, Budapest, Hungary^c; Department of Microbiology and Molecular Genetics, IMRIC, Faculty of Medicine, The Hebrew University of Jerusalem, Jerusalem, Israel^d; Department of Obstetrics and Gynecology, Hadassah University Hospital, and Faculty of Medicine, The Hebrew University of Jerusalem, Jerusalem, Israel^e

ABSTRACT Enteropathogenic *Escherichia coli* (EPEC) is a leading cause of severe intestinal disease and infant mortality in developing countries. Virulence is mediated by a type three secretion system (T3SS), causing the hallmark attaching and effacing (AE) lesions and actin-rich pedestal formation beneath the infecting bacteria on the apical surface of enterocytes. EPEC is a human-specific pathogen whose pathogenesis cannot be studied in animal models. We therefore established an EPEC infection model in human gut xenografts in SCID mice and used it to study the role of T3SS in the pathogenesis of the disease. Following EPEC O127:H6 strain E2348/69 infection, T3SS-dependent AE lesions and pedestals were demonstrated in all infected xenografts. We report here the development of T3SS-dependent intestinal thrombotic microangiopathy (iTMA) and ischemic enteritis in ~50% of infected human gut xenografts. Using species-specific CD31 immunostaining, we showed that iTMA was limited to the larger human-mouse chimeric blood vessels, which are located between the muscularis mucosa and circular muscular layer of the human gut. These blood vessels were massively invaded by bacteria, which adhered to and formed pedestals on endothelial cells and aggregated with mouse neutrophils in the lumen. We conclude that endothelial infection, iTMA, and ischemic enteritis might be central mechanisms underlying severe EPEC-mediated disease.

KEYWORDS EPEC, T3SS, human gut xenograft, mouse model, thrombotic microangiopathy

Enteropathogenic *Escherichia coli* (EPEC) is a leading cause of intestinal disease and infant mortality in developing countries (1, 2). Due to their high morbidity and mortality rates, EPEC infections represent an unmet challenge and a high research priority (3). Virulence is mediated by a type three secretion system (T3SS), causing the hallmark attaching and effacing (AE) lesions and actin-rich pedestal formation beneath the infecting bacteria on the apical surface of the epithelial cells lining the gut. EPEC is a human-specific pathogen, and despite impressive advances in our understanding of EPEC pathogenesis at the cellular and genetic levels, the pathophysiology of the resultant diarrhea and mortality remain unknown. Most of this advancing research has been carried out on *in vitro* model systems. However, the interplay of *in vivo* factors that

Received 3 August 2017 Accepted 4 August 2017

Accepted manuscript posted online 7 August 2017

Citation Nissim-Eliraz E, Nir E, Shoval I, Marsiano N, Nissan I, Shemesh H, Nagy N, Goldstein AM, Gutnick M, Rosenshine I, Yagel S, Shpigel NY. 2017. Type three secretion system-dependent microvascular thrombosis and ischemic enteritis in human gut xenografts infected with enteropathogenic *Escherichia coli*. *Infect Immun* 85:e00558-17. <https://doi.org/10.1128/IAI.00558-17>.

Editor Andreas J. Bäuml, University of California, Davis

Copyright © 2017 American Society for Microbiology. All Rights Reserved.

Address correspondence to Nahum Y. Shpigel, nahum.shpigel@mail.huji.ac.il.

result in diarrhea and neonatal mortality is very complex, and *in vitro* experiments yield only limited results (4). Moreover, the relevance of elucidating EPEC virulence mechanisms and their function during human infection can be validated only through clinical studies in human infants (5). We have therefore set as our first aim the establishment of an EPEC infection model using human gut xenografts in SCID mice. We selected prototypic EPEC strain E2348/69 O127:H6, which was originally isolated from an outbreak of infant diarrhea and thereafter has been used in human experimental infection studies (6, 7). We report here the establishment of a model of EPEC infection in the pediatric human gut which recapitulates the hallmark AE lesions and pedestal formation. Moreover, infection was also associated with manifestations of disease and pathological changes that might have been overlooked in clinical cases. A better understanding of the pathophysiology of EPEC infection in the pediatric human gut might lead to the development of improved therapeutic approaches to this serious disease.

RESULTS

***In vitro* system validation.** T3SS activity in EPEC wild-type (WT) organisms and a lack of activity in the Δ escV mutant were verified *in vitro*. While localized adherence and microcolonies were formed by both strains (see Fig. S1 and S2 in the supplemental material), pedestals of polymerized actin were visible only under EPEC WT bacteria infecting EPH4 cells (Fig. S1).

Attaching and effacing lesions, pedestal formation, and inflammation in infected human gut xenografts. The mean incubation period observed following experimental challenge studies in humans was \sim 8 h, and this was therefore selected as an endpoint in the present study. The challenge dose used in human studies was 10^{10} CFU; this was reduced to 10^7 CFU to accommodate the smaller size of the human pediatric gut model system (6, 7). Next, the EPEC infection model system was optimized to achieve colonization of the mucosal epithelial cells showing the typical attaching and effacing (AE) lesions and pedestal formation 8 h after intraluminal injection of $\sim 10^7$ CFU (Fig. 1A to E). Consistent with our *in vitro* observation, the Δ escV mutant strain formed microcolonies locally adherent to the microvilli on the apical membrane of enterocytes (Fig. 1F) but was unable to form AE lesions and pedestals. Furthermore, our experimental system clearly demonstrates that bacteria associated with AE lesions accounted for only a minor fraction of the total number of intestinal EPEC bacteria. The formation of AE lesions in the intact tissue within 8 h after infection was very infrequent. We could detect it in only a few percent of the tested sections of a given infected transplant (\sim 1 to 5%). Similarly, duodenal biopsy specimens obtained from diarrheic adult volunteers 24 h after experimental EPEC infection appeared histologically normal, and no bacteria were detected (7). Therefore, effacing and the loss of gut epithelial microvilli are unlikely to be the key mechanisms of diarrhea observed in human patients. We concluded that EPEC infection of the human gut xenograft model system recapitulated the characteristic virulence mechanisms and pathological lesions previously reported *in vitro* and *in vivo*. Moreover, using quantitative PCR (qPCR) analysis of whole human gut xenografts, we showed increased relative expression of human (Fig. 2A) and mouse (Fig. 2B) cytokines, chemokines, and NF- κ B-dependent genes 8 h after infection with the EPEC WT or Δ escV mutant, with no significant difference existing between the two strains. We concluded that global gut inflammation was neither dependent on nor modulated by the T3SS. Inflammation was most probably activated by microbe-associated molecular patterns (MAMPs), such as lipopolysaccharide, lipoproteins, and flagellin, as previously reported from studies using the same model system (8, 9). Inflammation was not associated with leukocyte recruitment into the mucosal tissues or lumen of infected gut xenografts. These results correlate with those of experimental human infection studies demonstrating signs of gut disease and systemic immune response (anti-O127 antibodies) following oral challenge with EPEC O127:H6 strain E2348/69 and isogenic T3SS mutants

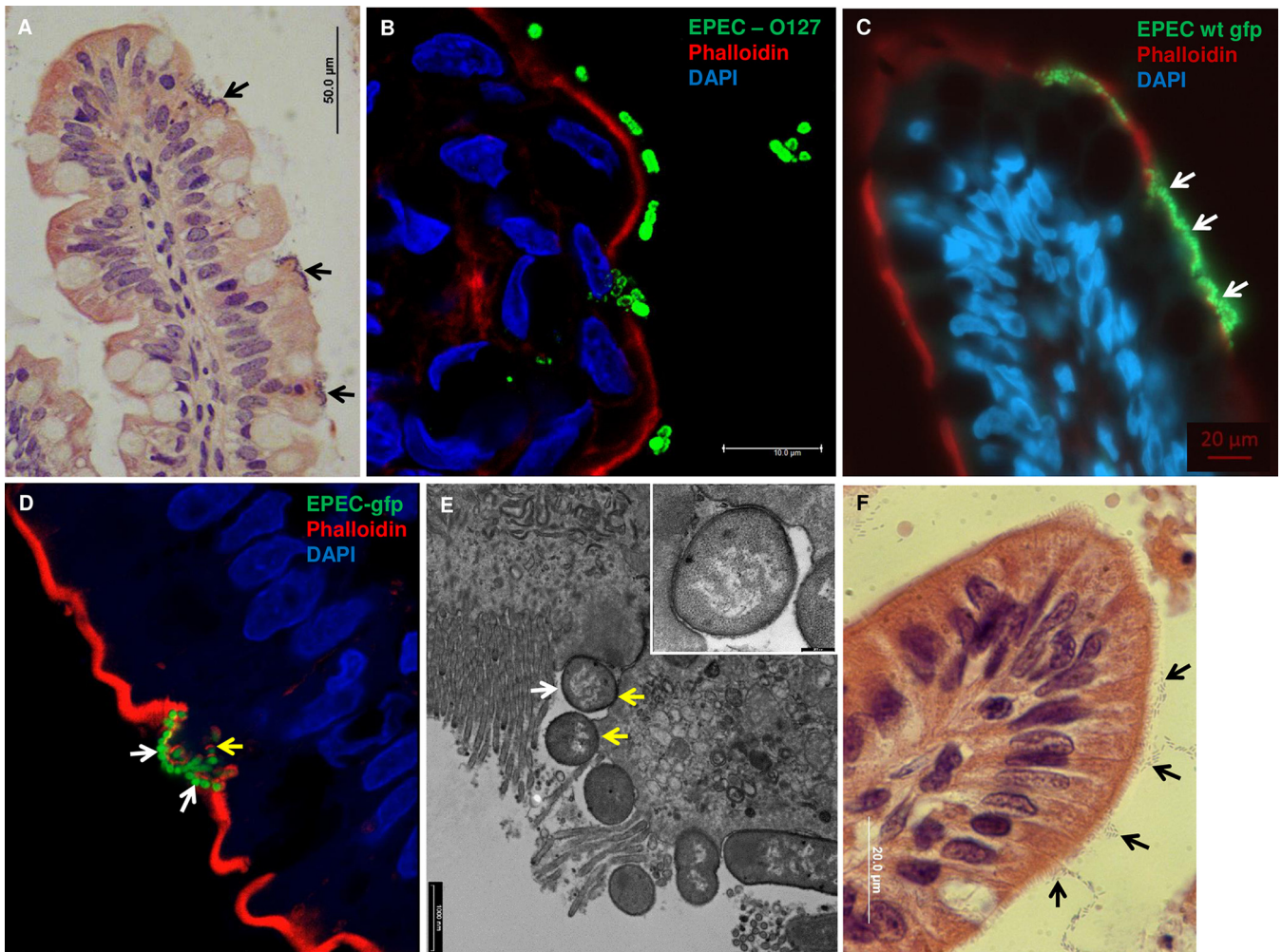


FIG 1 Attaching and effacing lesions and pedestal formation in EPEC-infected human gut xenografts. The interaction of EPEC O127 wild-type strain E2348/69 (A to E) and an isogenic Δ escV mutant strain (F) with human intestinal mucosa is shown. Foci of intimately adherent O127-positive bacteria were observed using H&E staining (A, black arrows), immunostaining (B), GFP-expressing bacteria (C and D, white arrows), and transmission electron microscopy (TEM) (E, white arrow). Pedestal formation under adherent bacteria and effacement of the brush border were demonstrated using confocal microscopy (showing a single Z-stack) (D, yellow arrow) and TEM (E, yellow arrows). Colonies of the T3SS-defective Δ escV mutant strain clustered on the brush border but were unable to form tight adhesion and effacement of the brush border (F, black arrows). Representative images of formalin-fixed paraffin-embedded H&E-stained sections (A and F) and fluorescence staining of cryosections using DAPI (B to D, blue) and phalloidin (B to D, red) are shown. Bars, 50 μ m (A), 10 μ m (B), 1,000 nm (E), 200 nm (E, inset), and 20 μ m (F). Magnification, $\times 63$ (C and D).

(6, 7). However, on the basis of analysis of gut biopsy and fecal specimens, these changes were not associated with leukocyte recruitment or tissue damage.

T3SS-dependent ischemic enteritis and microvascular thrombosis in infected human gut xenografts. Histopathological analysis of the human gut xenografts was performed 8 h after challenge with EPEC WT and Δ escV mutant organisms. Extensive lesions were observed in approximately 50% of infected xenografts (Fig. 3), whereas tightly adhering bacteria and AE lesions were visible in all infected xenografts. Pathological lesions in xenografts infected with the EPEC wild-type strain were characterized by well-demarcated areas of severe villous congestion (Fig. 3A and B) in association with epithelial sloughing and intact lamina propria, while villous outlines were well maintained (Fig. 3C to E, black arrows). The detachment of sheets of epithelial cells together from the villi is a known characteristic of acute gut ischemia (10). None of the xenografts infected with the Δ escV mutant organisms demonstrated the above-described pathological lesions, as indicated by the histological score (Fig. 3F). Both EPEC WT (Fig. 4A and B) and Δ escV mutant (Fig. 4C) organisms were visible in the submucosal venous blood vessels, and systemic dissemination was confirmed by

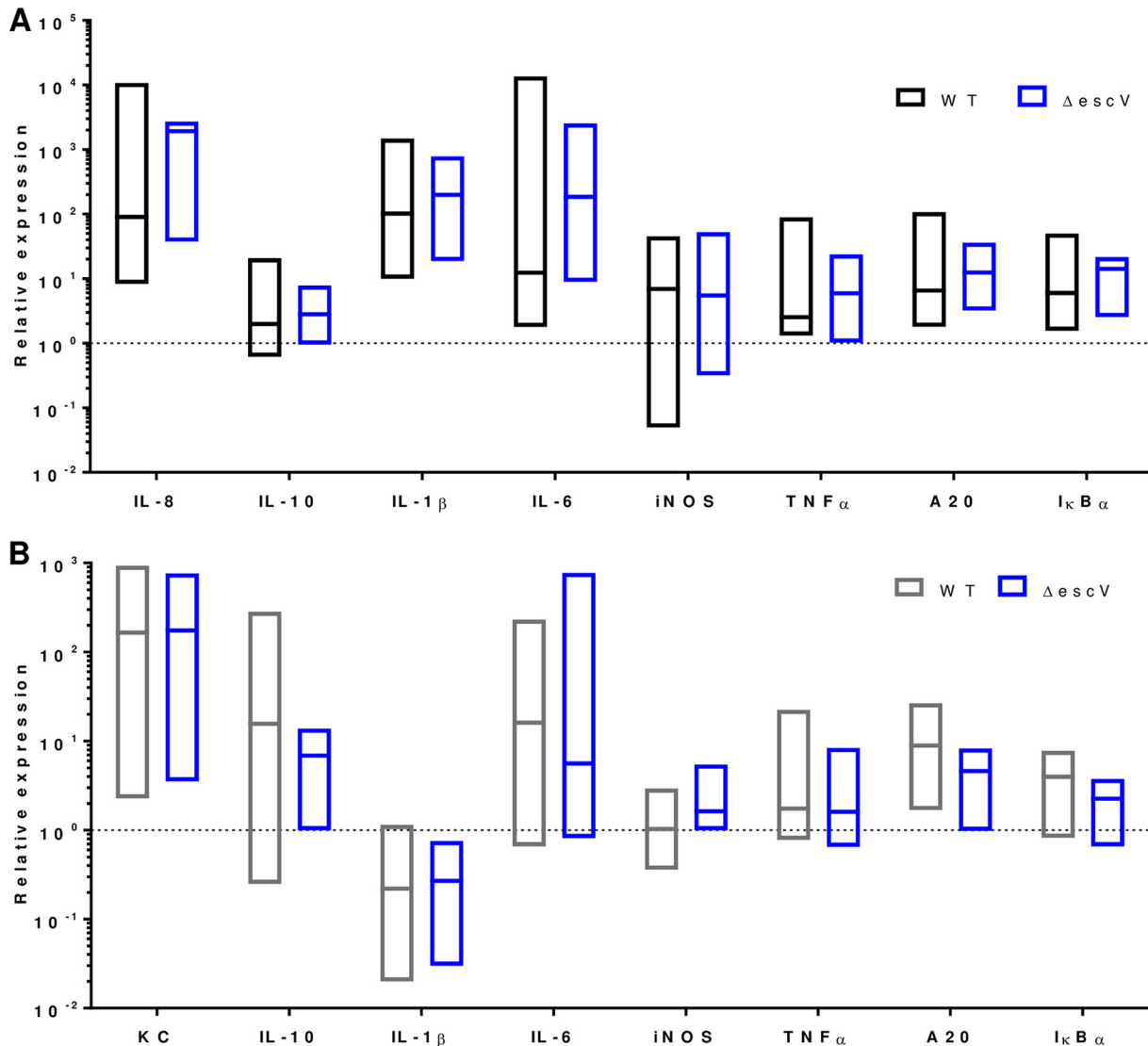


FIG 2 Markers of inflammation in EPEC-infected human gut xenografts. Elevated levels of expression of inflammatory markers in human gut xenografts were detected 8 h after infection with EPEC O127 wild-type strain E2348/69 and isogenic mutant strain $\Delta escV$. Species-specific quantitative real-time RT-PCR was used to measure the relative levels of expression of human (A) and mouse (B) cytokines, chemokines, and NF-kappa-B dependent genes in whole xenograft tissues. Expression levels were normalized against the levels for human $\beta 2$ -microglobulin (*B2M*) or mouse β -actin (*Actb*) mRNA and calculated relative to the expression levels for PBS-treated control xenografts using the $2^{-\Delta\Delta CT}$ method. Data are presented as ranges, and horizontal bars represent the medians. The differences between WT strain- and $escV$ mutant-infected xenografts were not statistically significant. IL-8, IL-10, IL-1 β , and IL-6, interleukins 8, 10, 1 β , and 6, respectively; iNOS, inducible nitric oxide synthase; TNF- α , tumor necrosis factor alpha; KC, keratinocyte-derived chemokine.

spleen cultures, with similar total counts being obtained for both strains (Fig. 4D). However, following EPEC WT infection, the submucosal blood vessels were also heavily congested with erythrocytes (RBCs) and neutrophils, forming large aggregates of neutrophils and bacteria (Fig. 4E and F and S3). The adherence of both EPEC WT (Fig. 4E and F) and $\Delta escV$ mutant (Fig. 4C) organisms to endothelial cells lining the blood vessels was clearly visible; however, actin pedestal formation was visible only under EPEC WT bacteria (Fig. 4F and S3). The above-described pathological changes elicited by EPEC WT organisms were consistently associated with microvasculature thrombosis (Fig. 5), leading to ischemic injury and necrosis of the villous epithelium with viable crypts. Histologically, the thrombi were limited to submucosal venous blood vessels located between the muscularis mucosa and circular muscles (Fig. 5A) and were constructed of fibrin and entrapped neutrophils and RBCs (Fig. 5B to D). Moreover, the presence of

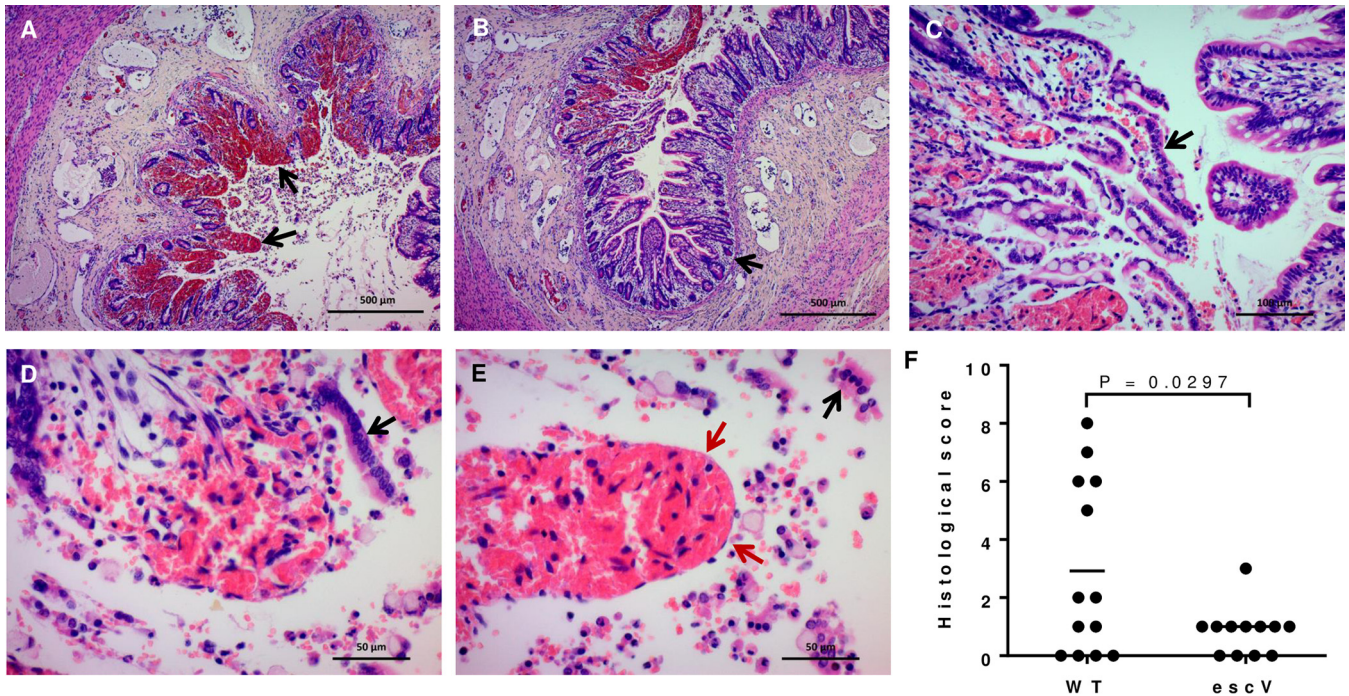


FIG 3 Ischemic enteritis in EPEC-infected human gut xenografts. Foci of ischemic enteritis in a human gut xenograft 8 h after infection with EPEC O127 strain E2348/69 bacteria are shown. Severe villous congestion is visible in a well-demarcated affected area (A, arrows), while the adjacent mucosa is not affected (B, arrow). Sheets of mucosal epithelial cells are sloughing and detaching (C to E, black arrows), leaving behind denuded outlines of congested villi (E, red arrows). (A to E) Representative images of formalin-fixed paraffin-embedded H&E-stained sections. (F) The scatter plot presents the histopathological scores for infected xenografts. Each data point represents a single xenograft. Mean scores (horizontal bars) were compared by an unpaired *t* test using GraphPad Prism (version 6) software (GraphPad Software, Inc.). A *P* value of 0.05 or less was considered significant. Bars, 500 μ m (A and B), 100 μ m (C), and 50 μ m (D and E).

submucosal thrombi was in perfect correlation with the high score for ischemic villous epithelial damage and congestion (histological score > 4).

We concluded that intestinal thrombotic microangiopathy (iTMA)-driven ischemic enteritis was T3SS dependent and might have been mediated by unknown perturbations of endothelial cell functions and the aggregation of blood neutrophils and bacteria.

Thrombosis is limited to submucosal human-mouse chimeric blood vessels.

The survival and normal development of the human fetal gut transplants are dependent on a blood supply from the mouse host. The extent and connectivity of the mouse and human vascular beds in the mature gut xenografts are unknown. Using species-specific anti-CD31 staining, we show here that the villous capillary networks were of human origin only (Fig. S4), while in the crypt zone we demonstrated two separate capillary networks of human and mouse origin (Fig. S5). The larger blood vessels in the submucosa were mostly of mouse origin; moreover, in this region we could demonstrate blood vessels lined by a mosaic of human and mouse endothelial cells (Fig. 6). Endothelial tightly adherent bacteria on actin pedestals, neutrophil aggregates (Fig. 4 and S3), and thrombosis (Fig. 5) were visible only in these human-mouse mosaic venous blood vessels, which were exclusively present in the submucosa. Taken together, these results suggest that it is likely that the development of thrombosis is linked to the formation of actin pedestals in the associated endothelium of the human-mouse mosaic blood vessels.

DISCUSSION

T3SS is considered the core virulence mechanism of EPEC, and AE lesions are the hallmark lesions associated with gut colonization and disease. There is general agreement among field experts that the destruction of microvilli by organisms causing AE lesions is the mechanism that underlies enteric disease and diarrhea (5). On the basis

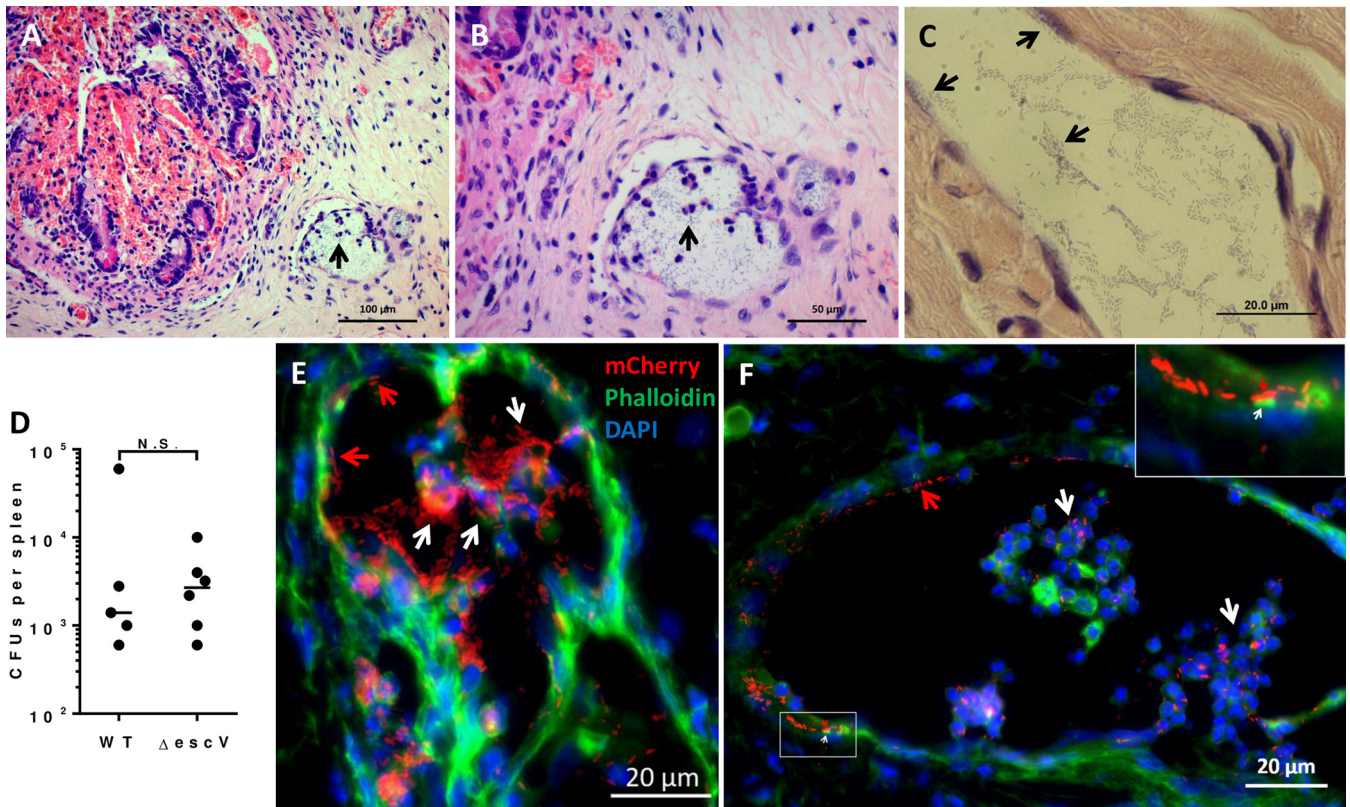


FIG 4 Submucosal vascular bacterial invasion and lesions. Local and systemic invasion of EPEC bacteria following infection of human gut xenografts is shown. (A to C) Both EPEC WT (black arrows in panel A and the magnified view in panel B) and $\Delta escV$ mutant (C) bacteria are visible in submucosal blood vessels. (D) Spleen tissue culture yielded similar bacterial cultures 8 h after challenge. (E and F) Only WT bacteria were associated with large aggregates of mouse neutrophils in the infected blood vessels (white arrows). Endothelial adherence of $escV$ mutant (C) and WT (E and F, red arrows) bacteria was clearly visible; however, actin pedestals (F and inset in panel F, white arrows) were visible only under WT bacteria adhering to endothelial cells lining the blood vessels. Representative images of formalin-fixed paraffin-embedded H&E-stained sections (A to C) and of cryosections that included mCherry-expressing bacteria (E and F, red) and that were stained with DAPI (E and F, blue) and phalloidin (E and F, green) are shown. Bars, 100 μm (A), 50 μm (B), and 20 μm (C, E, and F). See also Fig. S3 in the supplemental material.

of our observations in human gut xenografts and previously published human experimental infections (6, 7), AE lesions seem to be rare and are unlikely the mechanism of severe diarrhea and mortality associated with EPEC infection in infants (3). For many years EPEC has been considered a prototypic gut pathogen colonizing the mucosal surface. We show here that EPEC is able to traverse the mucosal barrier (known to be deranged by EPEC infection) and that the interaction of EPEC with vascular endothelial cells and blood neutrophils leads to thrombosis, congestion, and ischemic enteritis. Our results suggest that effector proteins introduced by T3SS into vascular endothelial cells might be the trigger of blood coagulation and thrombosis. Endothelial damage and altered expression of surface proteins are known to trigger blood coagulation, clotting, and thrombosis (11). To date, the effect of EPEC infection on human endothelial cells has not been studied and requires further consideration in future research. Interestingly, thrombotic microangiopathy of small blood vessels in the gut of infants dying of EPEC infection was described in older papers (12, 13). These lesions might have been overlooked and may contribute to the high rates of infant mortality associated with EPEC infection still prevalent in developing countries.

E. coli is known to cause intestinal thrombotic microangiopathy (iTMA) and hemorrhagic enteritis. Pathogenesis is most commonly attributed to the AB5 Shiga toxins Stx1 and Stx2 and the subtilase cytotoxin (SubAB) (14–16). We suggest here that although EPEC strains are not known to express these toxins (17), iTMA might be caused by an alternative mechanism which is T3SS dependent. One such mechanism could be the interaction of EPEC bacteria with host vascular endothelial cells. A second mechanism

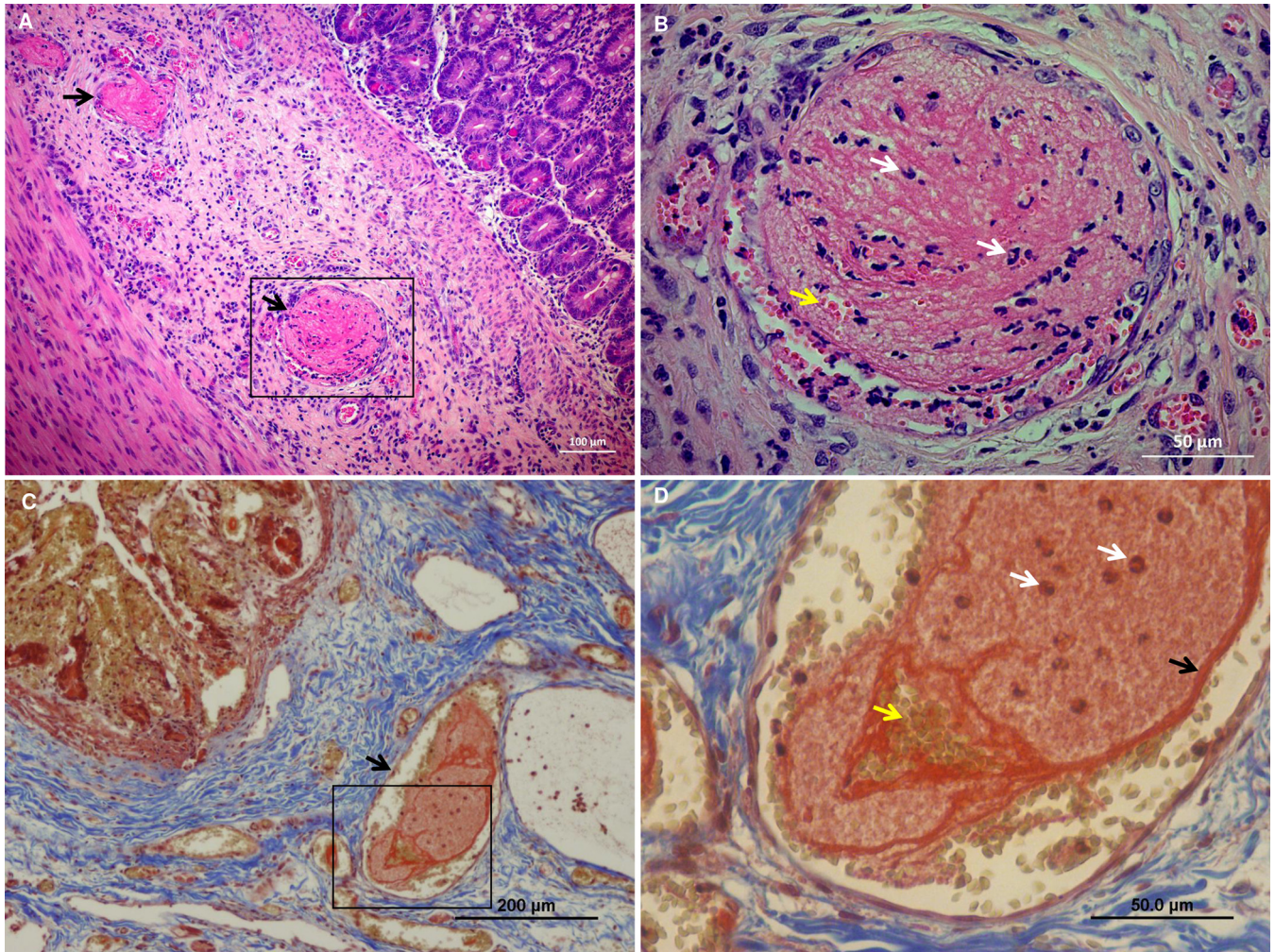


FIG 5 Intestinal thrombotic microangiopathy (iTMA). The thrombosis of submucosal blood vessels in human gut xenografts infected with EPEC O127 strain E2348/69 bacteria is shown. Multiple thrombi were visible in venous blood vessels between the muscularis mucosa and circular muscles of the human gut xenograft 8 h after infection with 10^7 CFU. (A and C) Vascular thrombosis was associated with severe villous congestion and ischemic necrosis of the mucosal epithelium, while the crypts were spared. Thrombi are visible in the boxed areas (A and C, arrows), which are better visible under the larger magnification in panels B and D. Thrombi consist of fibrin fibers (D, black arrow) entrapping numerous neutrophils (B and D, white arrows) and RBCs (B and D, yellow arrows). Representative images of formalin-fixed, paraffin-embedded, H&E-stained (A and B) and Masson's trichrome-stained (C and D) sections are shown. Bars, 100 μm (A), 50 μm (B and D), and 20 μm (C).

might be through interactions with blood neutrophils. We previously demonstrated a link between the activation of neutrophils by *E. coli* bacteria and the release of neutrophil extracellular traps (NETs) via a process called NETosis (18). This innate immune response is an effective bacterial clearance mechanism that involves the formation of an intravascular bactericidal net. NETosis has also been proposed to be a mechanism contributing to pathological microvascular thrombosis under septic disease conditions (19). However, although aggregates of mouse neutrophils and EPEC organisms were rampant in the gut microvasculature undergoing thrombosis, we were unable to demonstrate NETosis in this study.

In the model system used in the present study, transplants of human fetal gut develop into mature pediatric gut. We show here that EPEC infection of the pediatric human gut model can lead to severe pathological changes which are not explained by AE lesions and pedestal formation on enterocytes. The same EPEC strain used in this study was recently used to infect wild-type and immune-deficient neonatal and young mice. Interestingly, although the infecting organisms were able to produce typical AE lesions and pedestals in the neonatal mouse gut, clinical and pathological changes

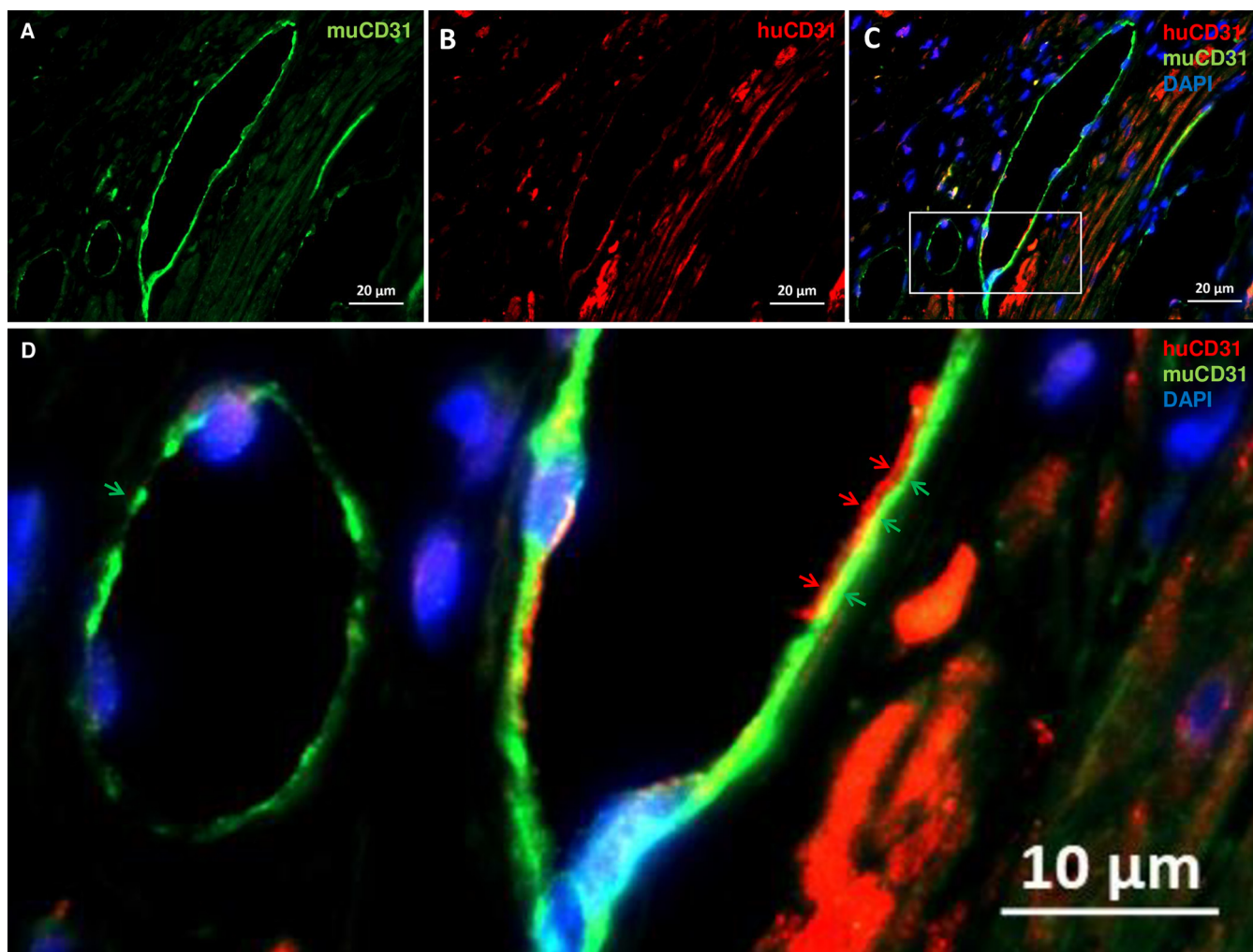


FIG 6 Submucosal human-mouse chimeric blood vessels. Submucosal venous blood vessels in human gut xenografts are comprised of anastomosing human and murine endothelial cells. Representative images of formalin-fixed, paraffin-embedded sections stained with murine anti-CD31 (muCD31) (A, green) and human anti-CD31 (huCD31) (B, red) fluorescent antibodies and DAPI (C and D, blue). The boxed area in panel C is enlarged for better visualization of overlapping human (D, red arrows) and murine (D, green arrows) endothelial cells lining the blood vessels. Bars, 20 μm (A to C) and 10 μm (D).

were not observed (20). It is unlikely that differences in intestinal microbiota are responsible for the difference observed between the two model systems. It is more likely that the difference reflects fundamental differences in the molecular mechanisms of the human and mouse gut. Thus, the development of the human fetal gut into the pediatric gut in SCID host mice is a unique model system that enables us to unveil the pathogenesis and disease mechanisms of human-specific enteropathogens. Our model was found to be highly reproducible and specific in its ability to recapitulate natural infections by enteric pathogens like enterohemorrhagic *E. coli* (EHEC) O157:H7 (21) and the probable zoonotic pathogen *Mycobacterium avium* subsp. *paratuberculosis* (22). In the current study, we expanded our validation to EPEC. It is noteworthy that iTMA and ischemic changes have also been described in the neonatal gut disease necrotizing enterocolitis (NEC), which affects premature infants. However, in NEC, iTMA was found in submucosal arterioles and led to coagulative necrosis of the mucosal epithelium (23, 24), while we describe here iTMA of the submucosal venules and ischemic necrosis of the villous epithelium, with iTMA sparing the crypts. Recent work has implicated uropathogenic *E. coli* (UPEC) colonization of the immature neonatal gut to be a significant risk factor for the development of NEC and subsequent mortality (25). The cause of NEC is not clear, and there is no specific test for early identification. The current

diagnostic tests, which entail biochemical and imaging techniques, are not sufficiently specific, nor are they sensitive enough (26). Moreover, progress in NEC research is hampered by the lack of an appropriate animal model. In conclusion, the human gut xenograft model offers a unique system to study human-specific gut pathology, including coagulopathies associated with colonization by strains of *E. coli*, as shown in this report.

MATERIALS AND METHODS

SCID mouse human intestinal xenotransplant models. C.B-17/lcrHsd-Prkdcscid (abbreviated SCID) mice were purchased from Harlan Biotech Israel (Rehovot, Israel). All mice were housed in a pathogen-free facility in individually ventilated cages (IVC) and given autoclaved food and water.

Human fetal small bowel (gestational age, 12 to 18 weeks) was implanted subcutaneously on the dorsum of the mouse as described previously (21, 22, 27). All surgical procedures were performed in an aseptic working environment in a laminar-flow HEPA-filtered hood with isoflurane inhalation anesthesia (1.5 to 2% [vol/vol] isoflurane in O₂). Before surgery, carprofen (5 mg/kg of body weight; Rimadyl; Pfizer Animal Health) was administered subcutaneously. The surgical area was shaved and depilated (with Nair hair removal cream), and the skin was scrubbed and disinfected with Betadine and 70% (vol/vol) ethanol.

After surgery the mice were provided with enrofloxacin-medicated water (Bayer Animal HealthCare AG) for 7 days and were closely monitored once a day for behavior, reactivity, appearance, and defecation. The grafts developed *in situ* for 12 to 16 weeks prior to manipulation.

This study was carried out in strict accordance with the recommendations for the care and use of laboratory animals of the National Institutes of Health. All procedures including animal studies were conducted following the guidelines for the care and use of laboratory animals of the Israel Ministry of Health and in accordance with Israeli law. The protocol was approved by the Animal Care and Use Committee (IACUC) of the Hebrew University of Jerusalem. Institutional review board (IRB) and IACUC approvals were obtained prospectively (Ethics Committee for Animal Experimentation, Hebrew University of Jerusalem [approval MD-11-12692-4] and the Helsinki Committee of the Hadassah University Hospital [approval 81-23/04/04]). Women undergoing legal terminations of pregnancy gave written, informed consent for the use of fetal tissue in this study.

Cells, bacteria, and plasmids. EPEC serotype O127:H6 wild-type (WT) strain E2348/69 (28) and its Δ escV mutant (the *escV* deletion caused inactivation of the T3SS) (29) were used in this study. Plasmid pSA11 carrying *lacI* and the green fluorescent protein (GFP) gene (*gfp*) or the mCherry gene (*cherry*) gene under the regulation of the *tac* promoter was introduced into the indicated strain, and GFP or mCherry expression was achieved by isopropyl- β -D-1-thiogalactopyranoside (IPTG; Sigma, Israel) (30).

Bacteria were grown in Luria-Bertani (LB) broth at 27°C. For *in vivo* challenge studies, cultures were diluted to 10⁷ CFU in 100 μ l culture medium and injected into the lumen of the human gut xenografts. To enable fluorescence visualization of the infecting bacteria, 100 μ l of 10 mM IPTG solution in phosphate-buffered saline (PBS) was injected into the lumen of the infected xenografts 1 h before mice were sacrificed for tissue harvesting. For enumeration of the bacteria in spleen, the organ was homogenized in 1 ml of PBS. Serial dilutions of the homogenates were plated onto LB agar, and the number of CFU was determined after overnight incubation at 37°C. The detection limit of the CFU assay was <10² CFU per spleen.

***In vitro* EPEC infection of mammary epithelial cells.** EPH4 murine mammary epithelial cells (kindly donated by B. Aroeti, Hebrew University) were cultured in Dulbecco's modified Eagle medium (DMEM) supplemented with 10% fetal calf serum (FCS) (Biological Industries) and 100 units/ml penicillin–0.1 mg/ml streptomycin (Pen-Strep; Biological Industries) at 37°C with 5% CO₂. The EPEC WT strain and the Δ escV mutant carrying a green fluorescent protein (GFP) expression plasmid were used for *in vitro* infection experiments. Cells were grown on 12-mm glass coverslips in 24-well plates (Nunc) overnight and were then infected with the EPEC WT strain or the *escV* mutant at a multiplicity of infection of 1 for 3 h. At 2 h after infection, IPTG was added to the culture medium at a final concentration of 0.1 mM. The slides were then fixed with 4% paraformaldehyde (PFA) and stained with phalloidin (Sigma) and 4',6'-diamidino-2-phenylindole (DAPI; Sigma). Coverslips were then mounted in mounting medium (Vectashield), and pictures were taken with an epifluorescence microscopy system (Axio Imager M1; Zeiss, Germany). Confocal images were acquired using a Leica Microsystems TCS SP2 laser-scanning spectrum confocal system, and images were merged using Leica confocal software.

Histochemical analysis. Mice were killed 8 h after challenge, and xenograft tissues were removed for histology, fluorescence staining, electron microscopy, and total bacterial counts. Samples for histological analysis were fixed in neutral buffered 4% PFA and embedded in paraffin, and sections were cut at a thickness of 5 μ m and stained with hematoxylin and eosin (H&E) or Masson's trichrome according to standard procedures.

Fresh xenograft tissue for fluorescence staining was fixed in 2.5% PFA overnight at room temperature, incubated with 15% (wt/vol) sucrose for 12 h at 4°C, and frozen in Tissue-Tek embedding medium (Electron Microscopy Sciences, Hatfield, PA). Serial 10- μ m cryosections were stained with phalloidin (Sigma) and DAPI (Sigma).

Staining of an EPEC O-antigen type strain was performed using rabbit anti-O127 (Statens Serum Institute, Denmark), and goat anti-rabbit IgG (catalog number ASF488; Invitrogen) was used as the secondary antibody. Endothelial cells were stained with rabbit anti-human CD31 (catalog number EPR3094; Abcam) and rat anti-murine CD31 (clone SZ31; Dianova, Hamburg, Germany). Donkey anti-rabbit immunoglobulin conjugated with Alexa Fluor 546 (catalog number A10040) and donkey anti-rat

immunoglobulin conjugated with Alexa Fluor 488 (catalog number A21208) (both from Life Technologies) were used as secondary antibodies.

Sections were mounted with Vectashield mounting medium (Vector Laboratories, Burlingame, CA) and imaged with an Axio Imager M1 upright fluorescence microscope (Zeiss, Germany). Confocal images were acquired using a Leica Microsystems TCS SP2 laser-scanning spectrum confocal system, and images were merged using Leica confocal software.

TEM. Samples for transmission electron microscopy (TEM) were fixed with a mixture of 2.5% glutaraldehyde in 0.1 M phosphate buffer, pH 7.2, for 2 h and then washed with 0.1 M phosphate buffer. After osmification, dehydration, and embedding (Epon), the tissue was sectioned using an LKB-Ultratome 8800 III ultramicrotome and observed with a Tecnai 12 TEM (Phillips, Eindhoven, The Netherlands) equipped with a MegaView II charge-coupled-device camera and AnalySIS (version 3.0) software.

Intestinal villous injury scoring. Scoring of histopathology was done by an individual blind to the treatment using a validated scoring system. Three independent parameters were measured: villous ischemic damage (scores, 0 to 3 for no, slight, moderate, and severe damage, respectively), cellular infiltration (scores, 0 to 3 for no, slight, moderate, and severe infiltration, respectively), and congestion and hemorrhage (scores, 0 to 3 for none, slight, moderate, and severe congestion and hemorrhage, respectively).

Quantitative RT-PCR. Total RNA was isolated from gut xenograft tissue using a GenElute mammalian total RNA miniprep kit (Sigma, Rehovot, Israel) combined with an on-column DNase I digestion set (Sigma). Reverse transcription (RT) was performed using a qScript cDNA synthesis kit (Quanta Biosciences, Gaithersburg, MD, USA), and cDNA was used for subsequent real-time PCRs. Quantitative real-time RT-PCR was conducted on a StepOne Plus PCR instrument (Applied Biosystems) using Fast qPCR Universal master mix (Kappa Biosystems, Boston, MA, USA). Species-specific primer pairs specific for the target human and mouse genes used in this study were designed and are listed in Table S1 in the supplemental material. To avoid any cross talk, primers were designed to amplify specifically human or mouse transcripts. All reactions were performed in triplicate, and the gene expression levels for each amplicon were calculated using the $2^{-\Delta\Delta CT}$ threshold cycle (C_T) method (31), and the levels were normalized against those for human β_2 -microglobulin (*B2M*) or mouse β -actin (*Actb*) mRNA. Melting curve analysis was performed with each primer set to confirm amplification of a single product, and all amplicons were sequenced to ensure reaction specificity (data not shown).

Statistical analysis. Parametric data (clinical scores) and nonparametric data (relative levels of expression of genes and CFU counts) were calculated as the mean and median, respectively. For comparison of parametric and nonparametric data, a *t* test and a nonparametric Mann-Whitney two-independent-samples test, respectively, were applied using GraphPad Prism (version 6) software (GraphPad Software, Inc.). A *P* value of 0.05 or less was considered significant.

SUPPLEMENTAL MATERIAL

Supplemental material for this article may be found at <https://doi.org/10.1128/IAI.00558-17>.

SUPPLEMENTAL FILE 1, PDF file, 0.7 MB.

SUPPLEMENTAL FILE 2, PDF file, 0.2 MB.

ACKNOWLEDGMENTS

We thank John Leong of Tufts University for helpful suggestions and encouragement.

NIH grant R21 AI107587 to Nahum Y. Shpigel and Ilan Rosenshine supported this work. Nahum Y. Shpigel, Allan M. Goldstein, and Michael Gutnick were supported by BSF grant 2015157. The work leading to the results presented here has received funding from the European Union Seventh Framework Programme (FP7/2012-2017) under grant agreement no. 305564 as a partner of the SysMedIBD Research Consortium (to Werner Muller, University of Manchester, Manchester, United Kingdom).

The funders had no role in study design, data collection and interpretation, or the decision to submit the work for publication.

REFERENCES

- Hazen TH, Donnenberg MS, Panchalingam S, Antonio M, Hossain A, Mandomando I, Ochieng JB, Ramamurthy T, Tamboura B, Qureshi S, Quadri F, Zaidi A, Kotloff KL, Levine MM, Barry EM, Kaper JB, Rasko DA, Nataro JP. 2016. Genomic diversity of EPEC associated with clinical presentations of differing severity. *Nat Microbiol* 1:15014. <https://doi.org/10.1038/nmicrobiol.2015.14>.
- Ochoa TJ, Contreras CA. 2011. Enteropathogenic *Escherichia coli* infection in children. *Curr Opin Infect Dis* 24:478–483. <https://doi.org/10.1097/QCO.0b013e32834a8b8b>.
- Donnenberg MS, Finlay BB. 2013. Combating enteropathogenic *Escherichia coli* (EPEC) infections: the way forward. *Trends Microbiol* 21: 317–319. <https://doi.org/10.1016/j.tim.2013.05.003>.
- Chen HD, Frankel G. 2005. Enteropathogenic *Escherichia coli*: unravelling pathogenesis. *FEMS Microbiol Rev* 29:83–98. <https://doi.org/10.1016/j.femsre.2004.07.002>.
- Law RJ, Gur-Arie L, Rosenshine I, Finlay BB. 2013. In vitro and in vivo model systems for studying enteropathogenic *Escherichia coli* infections. *Cold Spring Harb Perspect Med* 3:a009977. <https://doi.org/10.1101/cshperspect.a009977>.
- Tacket CO, Sztein MB, Losonsky G, Abe A, Finlay BB, McNamara BP,

- Fantry GT, James SP, Nataro JP, Levine MM, Donnenberg MS. 2000. Role of EspB in experimental human enteropathogenic *Escherichia coli* infection. *Infect Immun* 68:3689–3695. <https://doi.org/10.1128/IAI.68.6.3689-3695.2000>.
7. Donnenberg MS, Tacket CO, James SP, Losonsky G, Nataro JP, Wasserman SS, Kaper JB, Levine MM. 1993. Role of the *eaeA* gene in experimental enteropathogenic *Escherichia coli* infection. *J Clin Invest* 92:1412–1417. <https://doi.org/10.1172/JCI116717>.
 8. Miyamoto Y, Iimura M, Kaper JB, Torres AG, Kagnoff MF. 2006. Role of Shiga toxin versus H7 flagellin in enterohaemorrhagic *Escherichia coli* signalling of human colon epithelium in vivo. *Cell Microbiol* 8:869–879. <https://doi.org/10.1111/j.1462-5822.2005.00673.x>.
 9. Wong ARC, Pearson JS, Bright MD, Munera D, Robinson KS, Lee SF, Frankel G, Hartland EL. 2011. Enteropathogenic and enterohaemorrhagic *Escherichia coli*: even more subversive elements. *Mol Microbiol* 80:1420–1438. <https://doi.org/10.1111/j.1365-2958.2011.07661.x>.
 10. Grootjans J, Lenaerts K, Buurman WA, Dejong CH, Derikx JP. 2016. Life and death at the mucosal-luminal interface: new perspectives on human intestinal ischemia-reperfusion. *World J Gastroenterol* 22:2760–2770. <https://doi.org/10.3748/wjg.v22.i9.2760>.
 11. Engelmann B, Massberg S. 2013. Thrombosis as an intravascular effector of innate immunity. *Nat Rev Immunol* 13:34–45. <https://doi.org/10.1038/nri3345>.
 12. Rozansky R, Rosenmann E, Ben-Ari Y, Sterk VV. 1964. Enteropathogenic *Escherichia coli* infections in infants during the period from 1957 to 1962. *J Pediatr* 64:521–527. [https://doi.org/10.1016/S0022-3476\(64\)80341-3](https://doi.org/10.1016/S0022-3476(64)80341-3).
 13. Drucker MM, Polliack A, Yeivin R, Sacks TG. 1970. Immunofluorescent demonstration of enteropathogenic *Escherichia coli* in tissues of infants dying with enteritis. *Pediatrics* 46:855–864.
 14. Croxen MA, Law RJ, Scholz R, Keeney KM, Wlodarska M, Finlay BB. 2013. Recent advances in understanding enteric pathogenic *Escherichia coli*. *Clin Microbiol Rev* 26:822–880. <https://doi.org/10.1128/CMR.00022-13>.
 15. Furukawa T, Yahiro K, Tsuji AB, Terasaki Y, Morinaga N, Miyazaki M, Fukuda Y, Saga T, Moss J, Noda M. 2011. Fatal hemorrhage induced by subtilase cytotoxin from Shiga-toxigenic *Escherichia coli*. *Microb Pathog* 50:159–167. <https://doi.org/10.1016/j.micpath.2011.01.002>.
 16. Wang H, Paton JC, Paton AW. 2007. Pathologic changes in mice induced by subtilase cytotoxin, a potent new *Escherichia coli* AB5 toxin that targets the endoplasmic reticulum. *J Infect Dis* 196:1093–1101. <https://doi.org/10.1086/521364>.
 17. Ingle DJ, Tauschek M, Edwards DJ, Hocking DM, Pickard DJ, Azzopardi KI, Amarasena T, Bennett-Wood V, Pearson JS, Tamboura B, Antonio M, Ochieng JB, Oundo J, Mandomando I, Qureshi S, Ramamurthy T, Hossain A, Kotloff KL, Nataro JP, Dougan G, Levine MM, Robins-Browne RM, Holt KE. 2016. Evolution of atypical enteropathogenic *E. coli* by repeated acquisition of LEE pathogenicity island variants. *Nat Microbiol* 1:15010. <https://doi.org/10.1038/nmicrobiol.2015.10>.
 18. Grinberg N, Elazar S, Rosenshine I, Shpigel NY. 2008. Beta-hydroxybutyrate abrogates formation of bovine neutrophil extracellular traps and bactericidal activity against mammary pathogenic *Escherichia coli*. *Infect Immun* 76:2802–2807. <https://doi.org/10.1128/IAI.00051-08>.
 19. Kimball AS, Obi AT, Diaz JA, Henke PK. 2016. The emerging role of NETs in venous thrombosis and immunothrombosis. *Front Immunol* 7:236. <https://doi.org/10.3389/fimmu.2016.00236>.
 20. Dupont A, Sommer F, Zhang K, Repnik U, Basic M, Bleich A, Kühnel M, Bäckhed F, Litvak Y, Fulde M, Rosenshine I, Hornef MW. 2016. Age-dependent susceptibility to enteropathogenic *Escherichia coli* (EPEC) infection in mice. *PLoS Pathog* 12:e1005616. <https://doi.org/10.1371/journal.ppat.1005616>.
 21. Golan L, Gonen E, Yagel S, Rosenshine I, Shpigel NY. 2011. Enterohaemorrhagic *Escherichia coli* induce attaching and effacing lesions and hemorrhagic colitis in human and bovine intestinal xenograft models. *Dis Model Mech* 4:86–94. <https://doi.org/10.1242/dmm.005777>.
 22. Golan L, Livneh-Kol A, Gonen E, Yagel S, Rosenshine I, Shpigel NY. 2009. *Mycobacterium avium* paratuberculosis invades human small-intestinal goblet cells and elicits inflammation. *J Infect Dis* 199:350–354. <https://doi.org/10.1086/596033>.
 23. Nankervis CA, Giannone PJ, Reber KM. 2008. The neonatal intestinal vasculature: contributing factors to necrotizing enterocolitis. *Semin Perinatol* 32:83–91. <https://doi.org/10.1053/j.semperi.2008.01.003>.
 24. McElroy SJ, Underwood MA, Sherman MP. 2013. Paneth cells and necrotizing enterocolitis: a novel hypothesis for disease pathogenesis. *Neonatology* 103:10–20. <https://doi.org/10.1159/000342340>.
 25. Ward DV, Scholz M, Zolfo M, Taft DH, Schibler KR, Tett A, Segata N, Morrow AL. 2016. Metagenomic sequencing with strain-level resolution implicates uropathogenic *E. coli* in necrotizing enterocolitis and mortality in preterm infants. *Cell Rep* 14:2912–2924. <https://doi.org/10.1016/j.celrep.2016.03.015>.
 26. Neu J. 2014. Necrotizing enterocolitis: the mystery goes on. *Neonatology* 106:289–295. <https://doi.org/10.1159/000365130>.
 27. Canavan JB, Scotta C, Vossenkamper A, Goldberg R, Elder MJ, Shoval I, Marks E, Stolarczyk E, Lo JW, Powell N, Fazekasova H, Irving PM, Sanderson JD, Howard JK, Yagel S, Afzali B, MacDonald TT, Hernandez-Fuentes MP, Shpigel NY, Lombardi G, Lord GM. 2016. Developing in vitro expanded CD45RA⁺ regulatory T cells as an adoptive cell therapy for Crohn's disease. *Gut* 65:584–594. <https://doi.org/10.1136/gutjnl-2014-306919>.
 28. Nataro JP, Kaper JB. 1998. Diarrheagenic *Escherichia coli*. *Clin Microbiol Rev* 11:142–201.
 29. Nadler C, Baruch K, Kobi S, Mills E, Haviv G, Farago M, Alkalay I, Bartfeld S, Meyer TF, Ben-Neriah Y, Rosenshine I. 2010. The type III secretion effector NleE inhibits NF- κ B activation. *PLoS Pathog* 6:e1000743. <https://doi.org/10.1371/journal.ppat.1000743>.
 30. Schlosser-Silverman E, Elgrably-Weiss M, Rosenshine I, Kohen R, Altuvia S. 2000. Characterization of *Escherichia coli* DNA lesions generated within J774 macrophages. *J Bacteriol* 182:5225–5230. <https://doi.org/10.1128/JB.182.18.5225-5230.2000>.
 31. Livak KJ, Schmittgen TD. 2001. Analysis of relative gene expression data using real-time quantitative PCR and the 2⁻($\Delta\Delta$ C_T) method. *Methods* 25:402–408. <https://doi.org/10.1006/meth.2001.1262>.